The Innovation

Article

Fast Evaporation Enabled Ultrathin Polymer Coatings on Nanoporous Substrates for Highly Permeable Membranes

Xiansong Shi,[1,3] Lei Wang,[1,3] Nina Yan,[1] Zhaogen Wang,[1] Leiming Guo,[2] Martin Steinhart,[2,*] and Yong Wang[1,*]
*Correspondence: martin.steinhart@uos.de (M.S.); yongwang@njtech.edu.cn (Y.W.)
Received: November 17, 2020; Accepted: January 31, 2021; Published Online: February 5, 2021; https://doi.org/10.1016/j.xinn.2021.100088

GRAPHICAL ABSTRACT

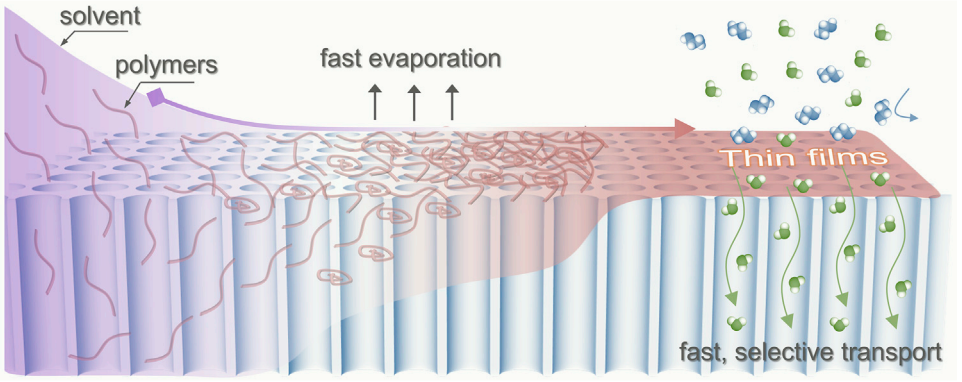

PUBLIC SUMMARY

- Fast solvent evaporation is developed to produce UPCFs on porous substrates
- Selective swelling to cavitate block copolymers to form interconnected mesopores
- UPCFs enable the preparation of highly permeable membranes

Article

Fast Evaporation Enabled Ultrathin Polymer Coatings on Nanoporous Substrates for Highly Permeable Membranes

Xiansong Shi,[1,3] Lei Wang,[1,3] Nina Yan,[1] Zhaogen Wang,[1] Leiming Guo,[2] Martin Steinhart,[2,*] and Yong Wang[1,*]

[1]State Key Laboratory of Materials-Oriented Chemical Engineering, College of Chemical Engineering, Nanjing Tech University, Nanjing, Jiangsu 211816, P.R. China

[2]Institut für Chemie neuer Materialien, Universität Osnabrück, Barbarastr. 7, 49069 Osnabrück, Germany

[3]These authors contributed equally

*Correspondence: martin.steinhart@uos.de (M.S.); yongwang@njtech.edu.cn (Y.W.)

Received: November 17, 2020; Accepted: January 31, 2021; Published Online: February 5, 2021; https://doi.org/10.1016/j.xinn.2021.100088

Citation: Shi X., Wang L., Yan N., et al., (2021). Fast Evaporation Enabled Ultrathin Polymer Coatings on Nanoporous Substrates for Highly Permeable Membranes. The Innovation **2(1)**, 100088.

Thin polymer coatings covering on porous substrates are a common composite structure required in numerous applications, including membrane separation, and there is a strong need to push the coating thicknesses down to the nanometer scale to maximize the performances. However, producing such ultrathin polymer coatings in a facile and efficient way remains a big challenge. Here, uniform ultrathin polymer covering films (UPCFs) are realized by a facile and general approach based on rapid solvent evaporation. By fast evaporating dilute polymer solutions spread on the surface of porous substrates, we obtain ultrathin coatings (down to ~30 nm) exclusively on the top surface of porous substrates, forming UPCFs with a block copolymer of polystyrene-*block*-poly(2-vinyl pyridine) at room temperature or a homopolymer of poly(vinyl alcohol) (PVA) at elevated temperatures. Upon selective swelling of the block copolymer and crosslinking of PVA, we obtain highly permeable membranes delivering ~2–10 times higher permeance in ultrafiltration and pervaporation than state-of-the-art membranes with comparable selectivities. We have invented a very convenient but highly efficient process for the direct preparation of defective-free ultrathin coatings on porous substrates, which is extremely desired in different fields in addition to membrane separation.

KEYWORDS: fast evaporation; ultrathin film; block copolymer; selective swelling; membrane separation

INTRODUCTION

The deposition of polymer solutions onto smooth solid substrates is a common route to produce polymer coatings, for example, protective layers or layers delivering specific functionalities, on a broad range of substrates. Established applications of polymer coatings lie in the fields of painting and printing,[1] biomedicine,[2] photovoltaics,[3] optoelectronics,[4] and membrane technology.[5,6] The substrates utilized in the abovementioned cases are mainly nonporous. If polymer solutions are applied to porous substrates, the nonvolatile polymer components are commonly penetrated into the substrate pores, resulting in undesired blocking that may affect the device performances.[7–10] Thus, concentrated polymer solutions with high viscosities are typically adopted for the preparation of polymer films on porous supports. For example, most microfiltration and ultrafiltration membranes were produced by the deposition of concentrated polymer solutions onto macroporous nonwoven fabrics followed by precipitation in water: nonsolvent-induced phase separation.[11] In this way, propagation of the polymer solutions into the pores of the nonwoven fabrics is retarded, but the permeance of thus-produced membranes is correspondingly sacrificed due to huge membrane thicknesses typically exceeding 100 μm.[12] To generate polymer coatings with thicknesses in the 10 μm range on porous substrates, the pores of the latter were prefilled with a liquid (typically water), followed by deposition of a polymer solution immiscible with the liquid prefilled in the substrate pores.[13–15] However, compared with ultrathin polymer films with thicknesses down to the nanometer scale, the polymer coatings with thicknesses in the 10–100 μm range exhibit great resistance to mass transfer. Therefore, ultrathin covering films with robust stability are always pursued to meet the demand of fast mass transport.[16–18] Particularly for membrane-based separations, the trade-off between selectivity and permeance significantly hampers the improvement of membrane performances.[19] Consequently, reducing the thickness of selective layers contributes to enhancing the permeance without sacrificing selectivity, thus possibly breaking the trade-off to promote the efficiency of membrane separations. Interfacial polymerization (IP) is a well-adapted strategy for the synthesis of ultrathin polymer films on porous supports[16,17]; however, IP is based on the ultrafast reactions between highly active monomers, and only very limited types of polymer films can be thus produced. Film transferring is considered as an alternative method to generate thin films on porous substrates, which has been used to produce composite structures toward diverse applications, including separation membranes.[20] Unfortunately, transferring becomes extremely difficult or even impossible if the film to be transferred is too thin in thickness or too large in lateral size. Hence, a facile yet effective strategy to directly build thin polymer films with thicknesses down to the nanometer scale on porous substrates still remains a big challenge.

The formation of covering films by coating solutions on porous substrates usually involves two competing processes, the Brownian motion of solutes and evaporation of solvents, determining the spatial distribution of the solute.[7] For instance, when the solvent evaporation dominates the process, the concentration gradient increases with the evaporation time, and the solute accumulates at the solution/air interface to form a thin coverage in the absence of infiltration. Undoubtedly, the final structure and solute distribution greatly depend on the evaporation rate of the solvent.[21] Therefore, we speculate that the control over the evaporation rate of the solvent, which can be easily realized in the experiment, may open up a new avenue to effectively govern the polymer distributions and film thicknesses, thus offering the possibility to engineer ultrathin polymer films with significantly decreased thicknesses on porous substrates.

Here, we report the preparation of ultrathin polymer covering films (UPCFs) enabled by fast evaporation of solvent and demonstrate their excellence as platforms for producing highly permeable membranes. Ultrafast evaporation of solvents induces the generation of a thin skin layer on anodic aluminum oxide (AAO) substrates, preventing the infiltration of solutes into substrate pores. With the subsequent treatments to as-prepared UPCFs, such as cavitation of block copolymers (BCPs) by selective swelling and crosslinking of poly(vinyl alcohol) (PVA), the resultant BCP and PVA membranes show excellent ultrafiltration and pervaporation performances characterized by high permeance at no or little expense of selectivity. Our findings establish a new platform to develop ultrathin covering films with diverse building blocks for ultrafast membrane separations.

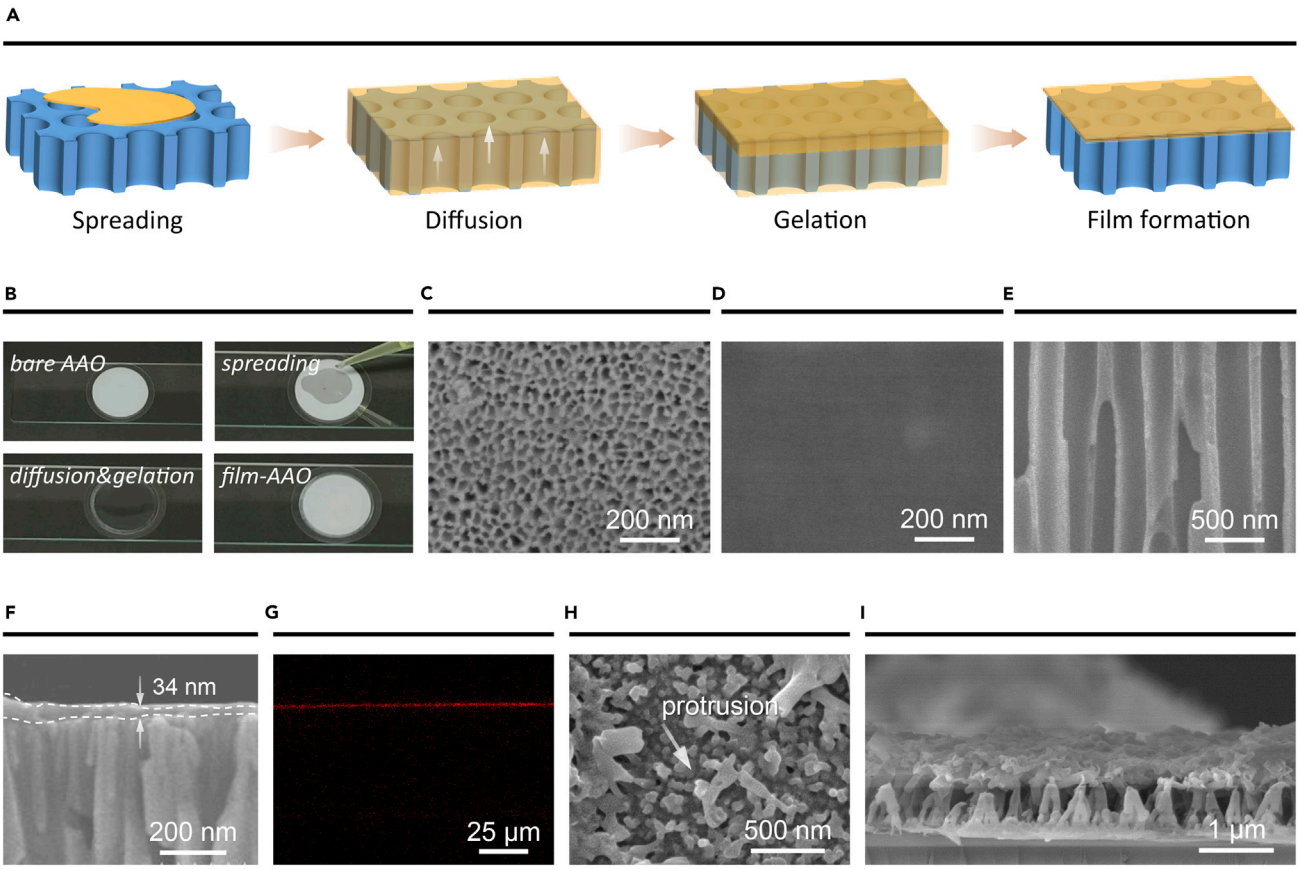

Figure 1. Fabrication of PS-*b*-P2VP UPCFs (A) Schematic diagram for the film preparation. (B) Digital images during the film preparation. (C and D) Surface SEM images of the bare AAO substrate and the UPCF. (E and F) Cross-sectional SEM images of the UPCF. (G) Cross-sectional fluorescent image. (H and I) Bottom and cross-sectional SEM images of the UPCF after removing AAO substrates. The UPCF was prepared by coating a 0.05 wt% PS-*b*-P2VP/CS_2 solution.

RESULTS AND DISCUSSION

The commercial AAO substrate utilized in this work consists of a thin size-selective layer of 100 nm thickness containing pores with a diameter of ~20 nm (hereafter referred to as a "size-selective AAO layer," Figure S1). The size-selective AAO layer is supported by a 60 μm thick AAO layer containing aligned cylindrical pores with diameters scattering about 200 nm. To prepare uniform and continuous UPCFs having thicknesses down to ~30 nm, we deposited dilute solutions of gelating polymers onto the size-selective AAO layers under conditions of fast solvent evaporation (Figure 1A). Thus, a bulk reservoir of the deposited solution covers the size-selective AAO layer from which the solvent evaporates. Diffusion processes in the solution are initially fast enough to prevent the occurrence of pronounced concentration gradients; the evaporation kinetics is determined by evaporative flux. Thereafter, mass transport slows down due to the progressing decrease in the solvent concentration. Solvent depletion at the evaporation surface is then no longer compensated by diffusion and a skin of the nonvolatile solutes forms at the solution surface.[22,23] Here, the formation of a polymer skin at the surface of the solution is also promoted by the evaporation-induced drop in temperature and by the tendency of the selected polymers to gelate. After complete solvent evaporation, the polymer skin is thus converted into a crack-free and continuous UPCF. The deposited polymer is mainly located in the UPCF while deposition of the polymer component into AAO pores is largely prevented.

We prepared UPCFs from the BCP of polystyrene-*block*-poly(2-vinyl pyridine) (PS-*b*-P2VP), which can easily be cavitated by selective swelling-induced pore generation so that mesoporous PS-*b*-P2VP-UPCFs (*m*UPCFs) are accessible.[24–27] Here, carbon disulfide (CS_2) was deliberately selected as the solvent due to its high volatility (vapor pressure 309 mm Hg at 21°C) and its low boiling point of 46.5°C.[28] Solutions of atactic PS in CS_2 are known to form unusually stable gels. Since atactic PS cannot crystallize, gelation is related to specific solvent-polymer interactions.[29,30] The PS is preferentially exposed to CS_2 as PS possesses a higher solubility in this solvent than P2VP.[31] One hundred-microliter portions of PS-*b*-P2VP/CS_2 solutions were spread on the size-selective AAO layers at 20°C ± 5°C (Figure 1B). The initially opaque AAO substrates immediately turned transparent, indicating fast imbibition. For a concentration of 0.05 wt% PS-*b*-P2VP, the AAO turned opaque again after ~70 s (Video S1), implying complete evaporation of CS_2 (Figure 1B, film-AAO). The fast evaporation of CS_2 is also revealed by recording the weight change during the evaporation (Figure S2). After coating a 0.05 wt% PS-*b*-P2VP/CS_2 solution, the obtained UPCF shows a smooth and continuous surface morphology, and no cracks, pinholes, or other defects are visible (Figure 1D). The dense structure contrasts sharply with the bare AAO substrate (Figure 1C). Moreover, the coating solution with a concentration of 0.03 wt% and 0.1 wt% is also applicable to form a crack-free UPCF (Figure S3). With the fast evaporation of CS_2, the PS-*b*-P2VP is predominantly located in the UPCF, demonstrated by the unimpeded pores without any blocking (Figures 1E and S4). The formed UPCFs exhibit tunable thicknesses in the range of ~30–215 nm, with the solution concentration increasing from 0.03 wt% to 0.1 wt% (Figures 1F and S5). The cross-sectional fluorescent image also demonstrates the formation of an ultrathin PS-*b*-P2VP film (Figure 1G). AAO substrates were then degraded to clearly observe the film structure, as shown in Figures 1H and 1I. Short protrusions with a length of ~650 nm exist on the bottom of PS-*b*-P2VP-UPCFs, which we interpret as negative replicas of the pore mouths of size-selective AAO layer.

Assuming that the porosity of AAO substrates amounts to 50%, the substrate correspondingly has an integrated pore volume of ~15 μL. Thus, 100 μL PS-*b*-P2VP/CS_2 solution ensures a complete filling of the AAO pores, and the excess solution forms a bulk reservoir covering the size-selective

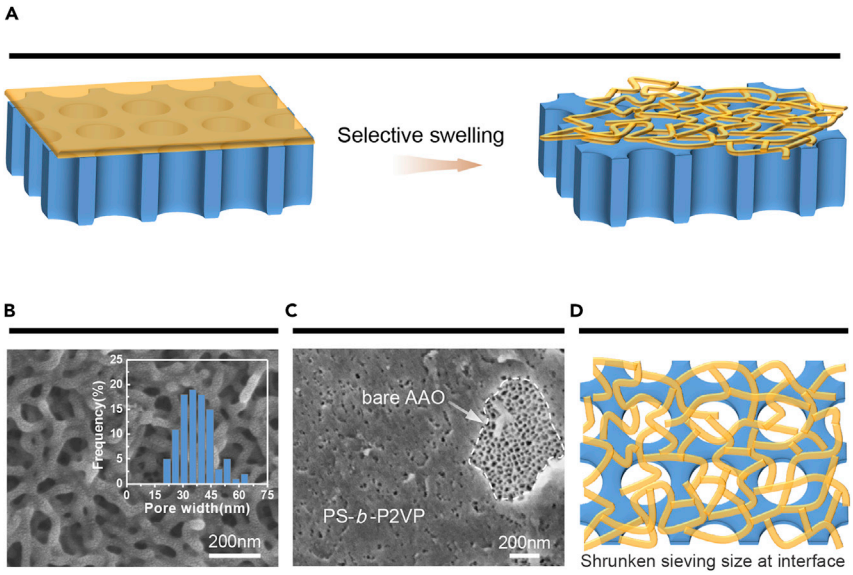

Figure 2. Selective Swelling of PS-*b*-P2VP-UPCF/AAO Composite Membranes (A) Schematic diagram of the selective swelling.
(B and C) Surface SEM images of the pristine and polished PS-*b*-P2VP-*m*UPCF/AAO membranes. The membrane was prepared with a 0.05 wt% precursor solution followed by swelling in 70°C ethanol for 1 h, and the inset in (B) shows the pore size distribution.
(D) Illustration of the shrunken sieving sizes induced by stagger stacking.

AAO layer. This speculation is also demonstrated by the appearance change of AAO during preparation, as discussed above. In this case, PS-*b*-P2VP should uniformly locate on the surface and entire pore walls of AAO substrate after CS_2 evaporation. Surprisingly, we can only observe a PS-*b*-P2VP film on the top layer of AAO substrates. The UPCF formation mechanism is given as follows. After solution spreading, the CS_2 evaporation will not only result in the depletion of the solvent and the enrichment of PS-*b*-P2VP at the solution surface, but also cause a drop in temperature. Rapid gelation of the PS blocks of PS-*b*-P2VP in the presence of CS_2, possibly superimposed by vitrification of PS and/or P2VP, will transform the solution from viscoelastic fluid to viscoelastic solid, generating a thin PS-*b*-P2VP skin that separates PS-*b*-P2VP/CS_2 solution from air.[7] Benefitting from the excellent compatibility between PS and CS_2, the succeeding evaporation of CS_2 is unobstructed with the existence of a PS-*b*-P2VP skin. Complete evaporation of the CS_2 transforms the thin PS-*b*-P2VP skin into a UPCF on the AAO substrate. Besides, during the infiltration of solution into AAO pores, irreversible adsorption of PS-*b*-P2VP molecules on the size-selective AAO layer may hinder further PS-*b*-P2VP molecules to enter the narrow AAO pore necks according to the findings reported by Karagiovanaki et al.[32] In addition, the fast evaporation of CS_2 rapidly increases the solution concentration, contributing to the immobilization of PS-*b*-P2VP on the top of AAO. These results synergistically lead to the generation of continuous films having short protrusions underneath them. The wetting of glass slides, which was used to hold AAO substrates, by CS_2 solution but no PS-*b*-P2VP on them demonstrates the proposed mechanism. Furthermore, considering that the adopted volatile solvent dominates the formation process of thin coverings, it is highly possible to directly prepare thin inorganic coatings on porous substrates for producing composite materials, which exhibit promising applications in diverse areas.

To convert nonporous PS-*b*-P2VP-UPCFs into *m*UPCFs, we introduce a nondestructive pore-making strategy: selective swelling (Figure 2A). Specifically, a PS-*b*-P2VP-UPCF prepared by deposition of a solution of 0.05 wt% PS-*b*-P2VP in CS_2 was treated in ethanol at 70°C for 1 h. Here, the selection of ethanol as the swelling agent is because it is a good solvent to P2VP but poor solvent to PS, leading to the selective swelling of P2VP domains. After immersing the nonporous PS-*b*-P2VP-UPCFs into hot ethanol, ethanol molecules will preferentially enrich in P2VP domains because of the strong interaction between them. Then, P2VP domains tend to swell and expand their volumes, and the volumetric expansion will inevitably cause the deformation of the PS matrix bringing about an increase in the film thickness. Upon the removal of the film from ethanol bath, the P2VP chains start to deswell and collapse with the evaporation of ethanol. Thanks to the glassy PS matrix, the spaces initially occupied by the expanded P2VP domains are well maintained, thus producing nanopores covered with P2VP chains.[27] Notably, *m*UPCFs swollen at different temperatures exhibit a similar structure, showing a continuous-spongy network of curved, interconnected PS-*b*-P2VP cylinders with a diameter of ~40 nm (Figures 2B, S6, and S7). Inspection of SEM images reveals that the *m*UPCFs contain continuous mesopore systems with diameters ranging from ~20 to ~60 nm. Although the size of these pores is larger than that of the size-selective AAO layer, the stagger stacking of porous PS-*b*-P2VP layers and AAO top layers at the interface gives a significantly reduced pore size, as shown in Figures 2C, 2D, and S8. Thus shrunken channels will promote the selectivity of the PS-*b*-P2VP-*m*UPCF/AAO composite membranes, and similar improvements in selectivity induced by the stagger stacking also can be found in other nanoporous materials, such as covalent organic frameworks stacked in the offset eclipsed fashion.[33,34] More importantly, the mesopores on both sides of the interface deliver a low resistance to solvent and solute, thus promising an enhanced selectivity without noticeably sacrificing permeance. Benefitting from the enrichment of hydrophilic P2VP on the membrane surface, as well as the cavitation, the water contact angle is reduced from 94° to 80° after selective swelling, giving a good wettability that favors water permeation (Figure S9). No obvious structural change can be observed after the ultrasonication treatment, demonstrating the stability of coating layers on substrates (Figure S10).

As shown in Figure 3A, the separation performance of PS-*b*-P2VP-*m*UPCF/AAO composite membranes is relatively robust against variations of the preparation conditions, including PS-*b*-P2VP concentrations, as well as swelling temperatures and durations. For instance, increasing the PS-*b*-P2VP concentration in the initially applied PS-*b*-P2VP/CS_2 solutions from 0.03 wt% to 0.1 wt% results in a moderate decrease in water permeance from ~1,275 to ~1,042 L m^{-2} h^{-1} bar^{-1}. Increasing the temperature during selective swelling leads to more pronounced cavitation of the *m*UPCFs and in turn to increased water permeance.[35] When the swelling temperature increases from 65°C to 75°C, the water permeance increases from ~915 to ~1,099 L m^{-2} h^{-1} bar^{-1}. Moreover, the swelling duration causes negligible influence on the water permeance. In all these cases, the rejections to bovine serum albumin (BSA) (M_w = 67 kDa) are >92% and remain nearly unchanged. It is worth noting that *m*UPCF/AAO composite membranes show tight rejections to proteins while they still exhibit a high water permeance of up to almost half the permeance of bare AAO substrates, which show no rejection to BSA. The *m*UPCF/AAO composite membrane also displays a rejection of ~95% and ~22% to ovalbumin (M_w = 45 kDa) and cytochrome *c* (M_w = 12.6 kDa), respectively, giving an approximatively molecular weight cut-off of ~42 kDa (Figure 3B). Apart from the abovementioned high porosities and stagger structures, this excellent separation performance may originate

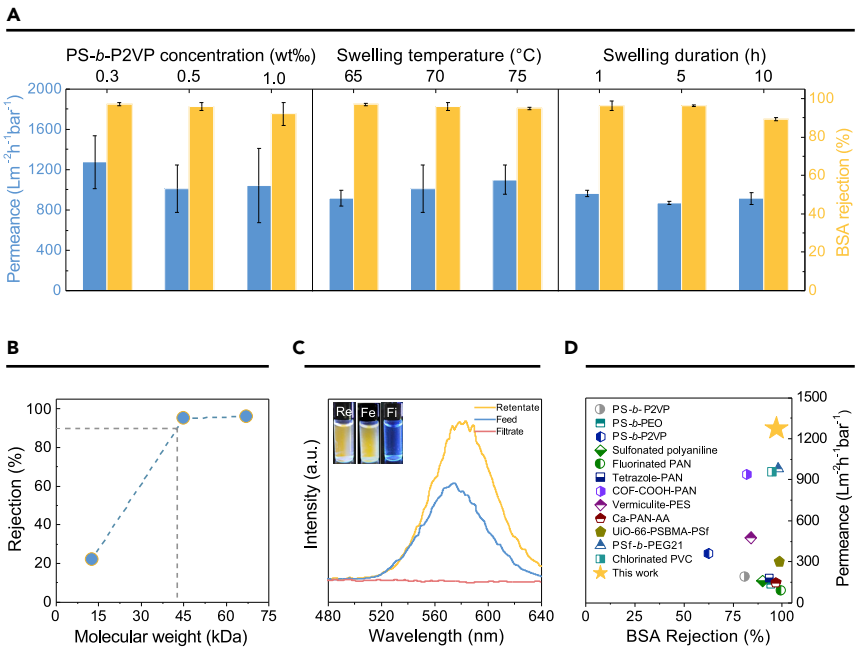

Figure 3. Separation Performance of PS-*b*-P2VP-*m*UPCF/AAO Composite Membranes (A) Performances with various PS-*b*-P2VP concentrations, swelling temperatures, and durations.
(B) Rejections to various objects with different molecular weights.
(C) Emission spectra of the feed, filtrate, and retentate obtained by concentrating CdTe QDs.
(D) Comparison on the separation performance of various membranes. Inset in (C) shows fluorescent photographs of the feed (Fe), filtrate (Fi), and retentate (Re). The results shown in (B–D) were obtained from the membrane prepared with a 0.05 wt% precursor solution followed by swelling in 70°C ethanol for 1 h.

from polar and water-permeable P2VP blocks as well.[36] Furthermore, the benefit of CS_2 adoption can be easily perceived by comparing the separation performances of membranes prepared with other solvents (Figure S11). Given the tight selectivity of our membranes, the resultant *m*UPCF/AAO composite membranes are applicable to recover valuable nanoparticles from water. As a demonstration, we implemented the concentration of CdTe quantum dots (QDs) with a diameter of 4 nm dispersed in water, as shown in Figure 3C. The emission spectrum of the QDs in feed shows a strong peak at ~570 nm and intense fluorescence signal (inset in Figure 3C). In contrast, the filtrate exhibits no peak and fluorescence signal, indicating a prominent repulsion of QDs by our membranes. The increased fluorescence of retentate reveals that the size sieving rather than adsorption plays a dominating role in the QDs recovery. Compared with our previously reported BCP-based membranes[26,37,38] and other membranes prepared by various materials,[39–47] the

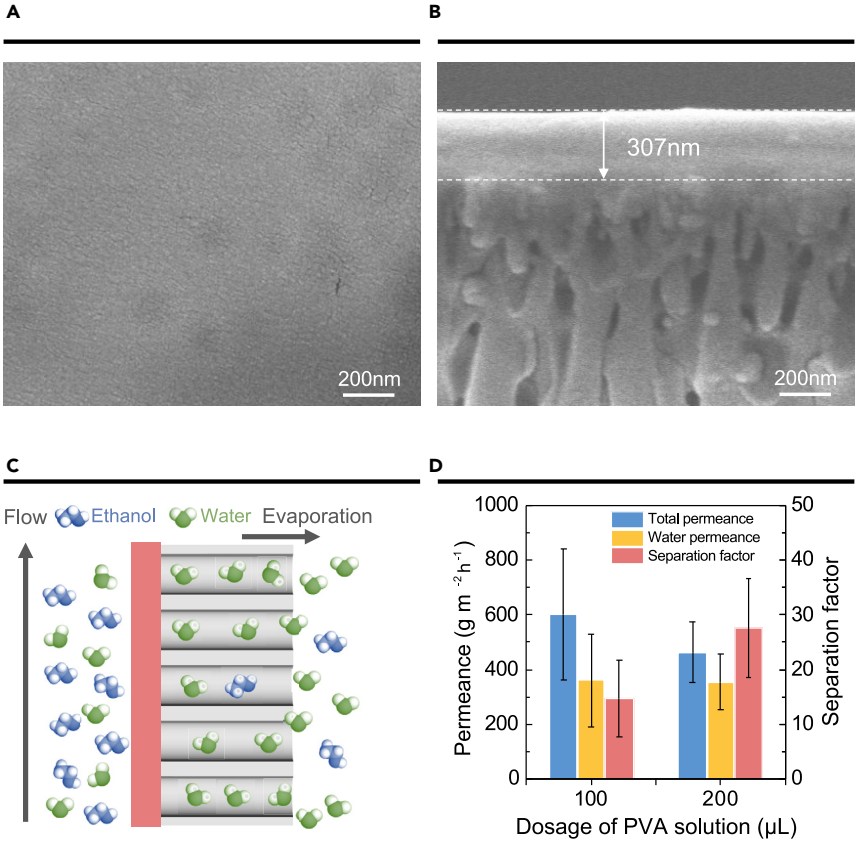

Figure 4. Crosslinked PVA-UPCF/AAO Composite Membranes for the Dehydration of Ethanol by Pervaporation
(A and B) Surface and cross-sectional SEM images of the membrane prepared with 100 μL PVA solution.
(C) Schematic diagram for the pervaporation.
(D) Permeance and separation factors of membranes prepared with various dosages of PVA solution.

PS-*b*-P2VP-*m*UPCF/AAO composite membranes show outstanding selectivities with ~2–10 times higher water permeance (Figure 3D), indicating their high efficiency for membrane-based separations, such as protein purification, nanoparticle concentration, and recovery of nano-sized precious metals from water.

Post-cavitation of dense PS-*b*-P2VP-UPCFs leads to mesoporous UPCFs that can be adopted for highly permeable ultrafiltration. Alternatively, as-coated dense UPCFs are considered as promising candidates for pervaporation through the solution-diffusion model.[48,49] To this end, we prepared crosslinked PVA-UPCFs for the recovery of ethanol from dilute aqueous solution. The rapid evaporation of solvent results in uniform and continuous PVA-UPCFs supported by AAO substrates (Figures 4A and 4B). The control over solution volume during coating enables a tunable film thickness. Concretely, we can obtain films with thicknesses of ~307 and ~585 nm when applying a solution volume of 100 and 200 μL, respectively. After crosslinking the PVA with maleic anhydride,[50] the dehydration performance of the obtained PVA-UPCF/AAO composite membranes were investigated. Taking advantage of the fact that water diffuses faster through PVA than ethanol,[51] we used PVA-UPCF/AAO composite membranes to concentrate water at the permeate side, as illustrated in Figure 4C. As a result, while the water content in the feed amounts to ~10 wt%, water is successfully concentrated to >75 wt% in the permeate after pervaporation through our membranes. The separation factor and the flux are determined to be 14.7 and 600 g m^{-2} h^{-1} for the PVA-UPCF/AAO composite membrane that resulted from 100 μL PVA solution (Figure 4D). Increasing the volume of the deposited PVA solution to 200 μL improves the separation factor to 27.6, while a high flux of 463 g m^{-2} h^{-1} is still retained. In terms of permeance, such dehydration performances are excellent compared with previously reported pervaporation membranes prepared by other methods.[52–54]

CONCLUSIONS

In conclusion, we have developed composite membranes that show multiple times higher permeance than state-of-the-art membranes while selectivities are comparable. The composite membranes consist of UPCFs with thicknesses down to a few 10 nm coated on porous substrates, anodic alumina membranes. The UPCFs form when diluted solutions of gel-forming polymers are deposited onto the substrates under conditions of fast solvent evaporation. As the solvent evaporates from the solution covering the substrates, the nonvolatile polymer solutes enrich at the solution surface. At advanced evaporation stages a thin layer of gelated and/or vitrified polymer forms as a skin on the polymer solution. After complete solvent evaporation, this skin eventually covers the porous substrate. To demonstrate the application of thus-produced structures, we prepared nanoporous ultrathin PS-*b*-P2VP covering films by deposition from solutions in CS_2 followed by selective swelling-induced pore generation. The combination of excellent selectivity and excellent permeance characterizing the composite membranes obtained in this way can be explained by a reduction of the effective pore size in the size-selective layer while efficient percolating pore networks are maintained. Crosslinked ultrathin PVA covering films showed excellent pervaporation performance as exemplarily demonstrated by the dehydration of ethanol. Moreover, the preparative approach reported here is a generic methodology to coat nanoporous substrates with ultrathin polymer films while avoiding polymer deposition into the substrate nanopores. This method is expected to find important applications in a diversity of fields.

REFERENCES

1. Callow, J.A., and Callow, M.E. (2011). Trends in the development of environmentally friendly fouling-resistant marine coatings. Nat. Commun. ***2***, 224.
2. Banerjee, I., Pangule, R.C., and Kane, R.S. (2011). Antifouling coatings: recent developments in the design of surfaces that prevent fouling by proteins, bacteria, and marine organisms. Adv. Mater. ***23***, 690–718.
3. Yan, Y., Liu, X., and Wang, T. (2017). Conjugated-polymer blends for organic photovoltaics: rational control of vertical stratification for high performance. Adv. Mater. ***29***, 1601674.
4. Han, D., Khan, Y., Ting, J., et al. (2017). Flexible blade-coated multicolor polymer light-emitting diodes for optoelectronic sensors. Adv. Mater. ***29***, 1606206.
5. Marchetti, P., Solomon, M.F.J., Szekely, G., and Livingston, A.G. (2014). Molecular separation with organic solvent nanofiltration: a critical review. Chem. Rev. ***114***, 10735–10806.
6. Lee, A., Elam, J.W., and Darling, S.B. (2016). Membrane materials for water purification: design, development, and application. Environ. Sci. Water Res. Technol. ***2***, 17–42.
7. Zhou, J., Man, X., Jiang, Y., and Doi, M. (2017). Structure formation in soft-matter solutions induced by solvent evaporation. Adv. Mater. ***29***, 1703769.
8. Martin, J., Maiz, J., Sacristan, J., and Mijangos, C. (2012). Tailored polymer-based nanorods and nanotubes by "template synthesis": from preparation to applications. Polymer ***53***, 1149–1166.
9. Chi, M.-H., Chang, C.-W., Ko, H.-W., et al. (2015). Solvent-induced dewetting on curved substrates: fabrication of porous polymer nanotubes by anodic aluminum oxide templates. Macromolecules ***48***, 6241–6250.
10. Steinhart, M., Zimmermann, S., Goring, P., et al. (2005). Liquid crystalline nanowires in porous alumina: geometric confinement versus influence of pore walls. Nano Lett. ***5***, 429–434.
11. Mulder, M. (2004). Basic Principles of Membrane Technology (Kluwer Academic Publishers).
12. Jana, S., Purkait, M.K., and Mohanty, K. (2011). Clay supported polyvinyl acetate coated composite membrane by modified dip coating method: application for the purification of lysozyme from chicken egg white. J. Membr. Sci. ***382***, 243–251.
13. Phillip, W.A., Amendt, M., O'Neill, B., et al. (2009). Diffusion and flow across nanoporous polydicyclopentadiene-based membranes. ACS Appl. Mater. Interfaces ***1***, 472–480.
14. Phillip, W.A., O'Neill, B., Rodwogin, M., et al. (2010). Self-assembled block copolymer thin films as water filtration membranes. ACS Appl. Mater. Interfaces ***2***, 847–853.
15. Jackson, E.A., Lee, Y., and Hillmyer, M.A. (2013). ABAC tetrablock terpolymers for tough nanoporous filtration membranes. Macromolecules ***46***, 1484–1491.
16. Gao, S., Zhu, Y., Gong, Y., et al. (2019). Ultrathin polyamide nanofiltration membrane fabricated on brush-painted single-walled carbon nanotube network support for ion sieving. ACS Nano ***13***, 5278–5290.
17. Karan, S., Jiang, Z., and Livingston, A.G. (2015). Sub-10 nm polyamide nanofilms with ultrafast solvent transport for molecular separation. Science ***348***, 1347–1351.
18. Yuan, J., Wu, M., Wu, H., et al. (2019). Covalent organic framework-modulated interfacial polymerization for ultrathin desalination membranes. J. Mater. Chem. A ***7***, 25641–25649.
19. Park, H.B., Kamcev, J., Robeson, L.M., et al. (2017). Maximizing the right stuff: the trade-off between membrane permeance and selectivity. Science ***356***, 1137.
20. Guio, L., Liu, C., Boures, D., et al. (2019). Procedure for the transfer of polymer films onto porous substrates with minimized defects. Jove, 59554.
21. Routh, A.F. (2013). Drying of thin colloidal films. Rep. Prog. Phys. ***76***, 046603.
22. Pauchard, L., and Allain, C. (2003). Buckling instability induced by polymer solution drying. Europhysics Lett. ***62***, 897–903.
23. Hennessy, M.G., Ferretti, G.L., Cabral, J.T., and Matar, O.K. (2017). A minimal model for solvent evaporation and absorption in thin films. J. Colloid Interface Sci. ***488***, 61–71.
24. Wang, Y., He, C., Xing, W., et al. (2010). Nanoporous metal membranes with bicontinuous morphology from recyclable block-copolymer templates. Adv. Mater. ***22***, 2068–2072.
25. Wang, Y., and Li, F. (2011). An emerging pore-making strategy: confined swelling-induced pore generation in block copolymer materials. Adv. Mater. ***23***, 2134–2148.
26. Shi, X., Wang, X., Wang, Y., and Wang, Y. (2020). Producing nanoporosities in block copolymers within 30 s by microwave-boosted selective swelling. Macromolecules ***53***, 3619–3626.
27. Zhou, J., and Wang, Y. (2020). Selective swelling of block copolymers: an upscalable greener process to ultrafiltration membranes? Macromolecules ***53***, 5–17.
28. Smallwood, I.M. (1996). Handbook of Organic Solvent Properties (John Wiley & Sons).
29. Tan, H.M., Moet, A., Hiltner, A., and Baer, E. (1983). Thermoreversible gelation of atactic polystyrene solutions. Macromolecules ***16***, 28–34.
30. Francois, J., Gan, J.Y.S., and Guenet, J.M. (1986). Sol-gel transition and phase-diagram of the system atactic polystyrene carbon-disulfide. Macromolecules ***19***, 2755–2760.
31. Cui, L., Xuan, Y., Li, X., et al. (2005). Polymer surfaces with reversibly switchable ordered morphology. Langmuir ***21***, 11696–11703.
32. Karagiovanaki, S., Koutsioubas, A., Spiliopoulos, N., et al. (2010). Adsorption of block copolymers in nanoporous alumina. J. Polym. Sci. B Polym. Phys. ***48***, 1676–1682.
33. Zhou, W., Wei, M., Zhang, X., et al. (2019). Fast desalination by multilayered covalent organic framework (COF) nanosheets. ACS Appl. Mater. Interfaces ***11***, 16847–16854.
34. Li, Y., Wu, Q., Guo, X., et al. (2020). Laminated self-standing covalent organic framework membrane with uniformly distributed subnanopores for ionic and molecular sieving. Nat. Commun. ***11***, 599.
35. Yan, N., and Wang, Y. (2015). Reversible switch between the nanoporous and the nonporous state of amphiphilic block copolymer films regulated by selective swelling. Soft Matter ***11***, 6927–6937.
36. Leson, A., Filiz, V., Foerster, S., and Mayer, C. (2007). Water permeation through block-copolymer vesicle membranes. Chem. Phys. Lett. ***444***, 268–272.
37. Yang, H., Wang, Z., Lan, Q., and Wang, Y. (2017). Antifouling ultrafiltration membranes by selective swelling of polystyrene/poly(ethylene oxide) block copolymers. J. Membr. Sci. ***542***, 226–232.

38. Wang, Y., Zhang, C., Zhou, J., and Wang, Y. (2020). Room-temperature swelling of block copolymers for nanoporous membranes with well-defined porosities. J. Membr. Sci. ***608***, 118186.
39. Zhao, X., and He, C. (2015). Efficient preparation of super antifouling PVDF ultrafiltration membrane with one step fabricated zwitterionic surface. ACS Appl. Mater. Interfaces ***7***, 17947–17953.
40. Zhao, X., Su, Y., Chen, W., et al. (2012). Grafting perfluoroalkyl groups onto polyacrylonitrile membrane surface for improved fouling release property. J. Membr. Sci. ***415***, 824–834.
41. Zhao, W., Liu, L., Wang, L., and Li, N. (2016). Functionalization of polyacrylonitrile with tetrazole groups for ultrafiltration membranes. RSC Adv. ***6***, 72133–72140.
42. Duong, P.H.H., Kuehl, V.A., Mastorovich, B., et al. (2019). Carboxyl-functionalized covalent organic framework as a two-dimensional nanofiller for mixed-matrix ultrafiltration membranes. J. Membr. Sci. ***574***, 338–348.
43. Orooji, Y., Liang, F., Razmjou, A., et al. (2017). Excellent biofouling alleviation of thermoexfoliated vermiculite blended poly(ether sulfone) ultrafiltration membrane. ACS Appl. Mater. Interfaces ***9***, 30024–30034.
44. Yang, Y., Li, X., Shen, L., et al. (2017). Ionic cross-linked poly(acrylonitrile-*co*-acrylic acid)/polyacrylonitrile thin film nanofibrous composite membrane with high ultrafiltration performance. Ind. Eng. Chem. Res. ***56***, 3077–3090.
45. Sun, H., Tang, B., and Wu, P. (2017). Development of hybrid ultrafiltration membranes with improved water separation properties using modified superhydrophilic metal-organic framework nanoparticles. ACS Appl. Mater. Interfaces ***9***, 21473–21484.
46. Wang, J., Liu, Y., Liu, T., et al. (2020). Improving the perm-selectivity and anti-fouling property of UF membrane through the micro-phase separation of PSf-*b*-PEG block copolymers. J. Membr. Sci. ***599***, 117851.
47. Liu, S., Chu, Y., Tang, C., et al. (2020). High-performance chlorinated polyvinyl chloride ultrafiltration membranes prepared by compound additives regulated non-solvent induced phase separation. J. Membr. Sci. ***612***, 118434.
48. Wijmans, J.G., and Baker, R.W. (1995). The solution-diffusion model: a review. J. Membr. Sci. ***107***, 1–21.
49. Guo, R., Fang, X., Wu, H., and Jiang, Z. (2008). Preparation and pervaporation performance of surface crosslinked PVA/PES composite membrane. J. Membr. Sci. ***322***, 32–38.
50. Xia, S., Dong, X., Zhu, Y., et al. (2011). Dehydration of ethyl acetate-water mixtures using PVA/ceramic composite pervaporation membrane. Sep. Purif. Technol. ***77***, 53–59.
51. Chen, J., Huang, J., Li, J., et al. (2010). Mass transport study of PVA membranes for the pervaporation separation of water/ethanol mixtures. Desalination ***256***, 148–153.
52. Wei, Y.M., Xu, Z.L., Qusay, F.A., and Wu, K. (2005). Polvvinvl alcohol/polysulfone (PVA/PSf) hollow fiber composite membranes for pervaporation separation of ethanol/water solution. J. Appl. Polym. Sci. ***98***, 247–254.
53. Hyder, M.N., Huang, R.Y.M., and Chen, P. (2008). Effect of selective layer thickness on pervaporation of composite poly(vinyl alcohol)-poly(sulfone) membranes. J. Membr. Sci. ***318***, 387–396.
54. Villagra Di Carlo, B., and Habert, A.C. (2013). Plasma-treated polyethersulfone coated with crosslinked poly(vinyl alcohol): composite membranes for pervaporation dehydration of ethanol. J. Mater. Sci. ***48***, 1457–1464.

ACKNOWLEDGMENTS

Financial support from the National Natural Science Fund for Distinguished Young Scholars (21825803) is gratefully acknowledged. We also thank the Program of Excellent Innovation Teams of Jiangsu Higher Education Institutions and the Project of Priority Academic Program Development of Jiangsu Higher Education Institutions (PAPD) for support. M.S. thanks the European Research Council (ERC-CoG-2014, project 646742 INCANA) and the German Research Foundation (INST 190/164-1 FUGG) for funding.

AUTHOR CONTRIBUTIONS

The manuscript was written through contributions of all authors. All authors have given approval to the final version of the manuscript. X.S. and L.W. contributed equally to this work.

DECLARATION OF INTERESTS

The authors declare no competing financial interest.

SUPPLEMENTAL INFORMATION

Supplemental Information can be found online at https://doi.org/10.1016/j.xinn.2021.100088.

LEAD CONTACT WEBSITE

funme.njtech.edu.cn